Spectral, Kinetic, and Thermodynamic Properties of Cu(I) and Cu(II) Binding by Methanobactin from *Methylosinus trichosporium* OB3b[†]

Dong W. Choi,[‡] Corbin J. Zea,[§] Young S. Do,[‡] Jeremy D. Semrau,[||] William E. Antholine,[⊥] Mark S. Hargrove,[‡] Nicola L. Pohl,[§,#] Eric S. Boyd,[@] G. G. Geesey,[@] Scott C. Hartsel,[+] Peter H. Shafe,[+] Marcus T. McEllistrem,[+] Clint J. Kisting,[‡] Damon Campbell,[+] Vinay Rao,[+] Arlene M. de la Mora,[¶] and Alan A. DiSpirito*[,‡]

Department of Chemistry and Plant Sciences Institute, and Psychology in Education Research Lab, Iowa State University, Ames, Iowa 50011-3211, Department of Civil and Environmental Engineering, University of Michigan, Ann Arbor, Michigan 48109-2125, Department of Biophysics, Medical College of Wisconsin, Milwaukee, Wisconsin 53226, Department of Microbiology, Montana State University, Bozeman, Montana 59717, and Department of Chemistry, University of Wisconsin, Eau Claire, Wisconsin 54702

Received September 8, 2005; Revised Manuscript Received December 2, 2005

ABSTRACT: To examine the potential role of methanobactin (mb) as the extracellular component of a copper acquisition system in *Methylosinus trichosporium* OB3b, the metal binding properties of mb were examined. Spectral (UV−visible, fluorescence, and circular dichroism), kinetic, and thermodynamic data suggested copper coordination changes at different Cu(II):mb ratios. Mb appeared to initially bind Cu(II) as a homodimer with a comparatively high copper affinity at Cu(II):mb ratios below 0.2, with a binding constant (K) greater than that of EDTA (log $K = 18.8$) and an approximate $\Delta G°$ of −47 kcal/mol. At Cu(II):mb ratios between 0.2 and 0.45, the K dropped to $(2.6 \pm 0.46) \times 10^8$ with a $\Delta G°$ of −11.46 kcal/mol followed by another K of $(1.40 \pm 0.21) \times 10^6$ and a $\Delta G°$ of −8.38 kcal/mol at Cu(II):mb ratios of 0.45−0.85. The kinetic and spectral changes also suggested Cu(II) was initially coordinated to the 4-thiocarbonyl-5-hydroxy imidazolate (THI) and possibly Tyr, followed by reduction to Cu(I), and then coordination of Cu(I) to 4-hydroxy-5-thiocarbonyl imidazolate (HTI) resulting in the final coordination of Cu(I) by THI and HTI. The rate constant (k_{obsI}) of binding of Cu(II) to THI exceeded that of the stopped flow apparatus that was used, i.e., >640 s^{-1}, whereas the coordination of copper to HTI showed a 6−8 ms lag time followed by a k_{obsII} of 121 ± 9 s^{-1}. Mb also solubilized and bound Cu(I) with a k_{obsI} to THI of >640 s^{-1}, but with a slower rate constant to HTI ($k_{obsII} = 8.27 \pm 0.16$ s^{-1}), and appeared to initially bind Cu(I) as a monomer.

Methanotrophs are characterized by their ability to utilize methane as a sole carbon and energy source (*1*). These cells are ubiquitous and play a major role in the global cycling of carbon and nitrogen as well as in the degradation of hazardous organic materials (*1*−*5*). In contrast to that for other bacteria, the copper requirement for methanotrophs expressing the membrane-associated or particulate methane monooxygenase (pMMO)[1] is severalfold higher than the organisms' iron requirements, and higher than that observed in other aerobic bacteria (*1*, *6*−*15*). In methanotrophs, copper has been shown to regulate expression of both the soluble and methane-associated methane monooxygenases, membrane development, and the expression of several other polypeptides that appear to be involved in either one-carbon metabolism, copper regulation, or copper transport (*8*−*11*, *15*−*21*). As methanotrophs have a high demand for copper, and copper has pleiotropic effects on methanotrophic physiology, these cells must have an effective mechanism for collecting copper. In fact, methanotrophs do appear to have a unique copper uptake system, similar to the siderophore-based iron uptake systems, utilizing a novel copper-binding chromopeptide called methanobactin (mb) (*11*, *15*, *22*−*24*).

Methanobactin (mb) is a small 1154 Da copper-binding chromopeptide initially identified in the methanotroph *Me-*

[†] This work was supported by Department of Energy Grant 02-96ER20237 (to A.A.D. and W.E.A.), an Inland Northwest research Alliance Graduate Fellowship grant to E.S.B., National Science Foundation Career Grant MCB 0349139 and Cottrell Awards (N.L.P.), and the Plant Sciences Institute and Department of Biochemistry, Biophysics and Molecular Biology for assistance in purchasing the isothermal titration calorimeter.

* To whom correspondence should be addressed. Telephone: (515) 294-2944. Fax: (515) 294-0453. E-mail: aland@iastate.edu.

[‡] Department of Biochemistry, Biophysics and Molecular Biology, Iowa State University.

[§] Department of Chemistry, Iowa State University.

[||] University of Michigan.

[⊥] Medical College of Wisconsin.

[@] Montana State University.

[+] University of Wisconsin.

[#] Plant Science Institute, Iowa State University.

[¶] Psychology in Education Research Lab, Iowa State University.

[1] Abbreviations: CD, circular dichroism; CT, charge transfer; Cu-mb, copper-containing methanobactin; Cu-s-mb, copper-stabilized methanobactin; EDTA-mb, Na_2EDTA-treated copper-stabilized mb; EPR, electron paramagnetic resonance; HTI, 4-hydroxy-5-thiocarbonyl imidazolate; Im, imidazole; ITC, isothermal titration calorimetry; mb, methanobactin; K, binding constant; k, rate constant; LMCT, ligand metal charge transfer; MLCT, metal ligand charge transfer; MMO, methane monooxygenase; pMMO, membrane-associated or particulate methane monooxygenase; THI, 4-thiocarbonyl-5-hydroxy imidazolate; XPS, X-ray photoelectron spectroscopy.

10.1021/bi051815t CCC: $33.50
Published on Web 01/10/2006 PAGE EST: 11.7

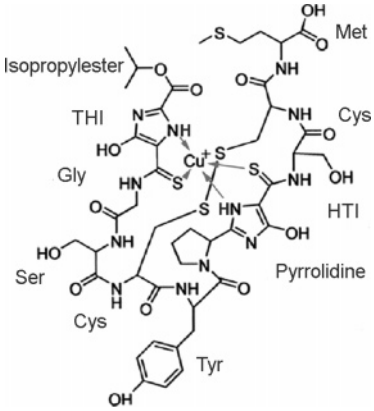

FIGURE 1: Schematic drawing of copper-containing methanobactin modified from ref *24*.

thylococcus capsulatus Bath during the isolation of the membrane-associated or particulate methane monooxygenase (pMMO) (*15*, *22*−*24*). Separation of copper-containing mb (Cu-mb) from pMMO results in the irreversible inactivation of the enzyme (*9*, *15*). Cu-mb has been shown to act as an oxygen radical scavenger and also to increase the rate of electron flow to the pMMO, but the involvement of Cu-mb in methane oxidation by the pMMO is still in question (*8*). In addition to the cytoplasmic membrane, mb has also been identified in the spent media of both *Mc. capsulatus* Bath and the type II methanotroph *Methylosinus trichosporium* OB3b (*15*, *22*, *25*). A number of studies have suggested mb acts as the extracellular component of a copper acquisition system (*11*, *15*, *22*−*26*). Last, it has been suggested that mb may serve as a copper chaperone for the pMMO or as a regulatory protein (*8*−*10*, *15*, *19*). Attempts to assign a single or distinct function to mb have proven unsuccessful, and taken together, these studies suggest mb may belong to a growing group of proteins known as "moonlighting proteins" (*27*−*32*). By definition, moonlighting proteins have the capacity to carry out two or more unrelated functions (*28*, *30*, *32*). The physiological functions of different moonlighting proteins vary with changes in cell location, oligomeric state, ligand or substrate concentration, change in physical environment, and/or complex formation with other proteins. Tompa et al. (*32*) have suggested that moonlighting proteins are intrinsically unstructured proteins, and it is this property that enables these proteins to have distinct functions. Consistent with other moonlighting proteins, gel filtration studies suggest mb will change conformation or form different oligomers at different Cu(II):mb ratios (*8*).

The crystal structure of copper-containing mb (Cu-mb) samples isolated following the exposure to copper concentrations in excess of 1000 Cu(II) atoms per mb has recently been determined (*23*, *24*) (Figure 1). The molecule exhibited some structural and spectral similarities to siderophores in the pyoverdin class (*33*, *34*). However, mb differed from this group of siderophores in amino acid composition and contained a biologically unique chromophore, 4-thiocarbonyl-5-hydroxy imidazolate (THI) or 4-hydroxy-5-thiocarbonyl imidazolate (HTI), each of which was responsible for copper coordination (*23*, *24*). In addition to copper coordination by THI and HTI moieties, the primary structure and amino acid composition of mb show other potential metal binding sites (*35*−*41*). Of particular interest to this study is the tyrosine-pyrrolidine group, which is structurally similar to tyrosine-proline. The phenoxide ion of Tyr has been shown to bind Cu(II), but ionization of Tyr generally occurs only at pH values around 10 (*42*). However, this ionization has been shown to occur at lower pH values in short peptide chains if Tyr is a terminal amino acid or if Pro is present (*40*, *41*). In mb, pyrrolidine structurally acts as a proline, providing a β-turn in the molecule (*24*). In addition, as observed in Pro, pyrrolidine does not possess an ionizable nitrogen, which can inhibit Cu(II) coordination by Tyr (*40*, *43*−*45*). Recent improvements in the isolation of low-copper-containing mb samples (*8*) allow for the first time examination of metal binding and solution properties of mb, and thus its potential role as a copper siderophore or chalkophore (*24*). The results presented here indicate mb is a dynamic molecule in solution and that the initial coordination of Cu(II) differs from the coordination observed in the final sample.

MATERIALS AND METHODS

Organism, Culture Conditions, and Isolation of Methanobactin. Ms. trichosporium OB3b was cultured in either 0 or 0.2 μM $CuSO_4$ amended nitrate minimal salts (NMS) medium as previously described (*9*). Mb, copper-containing mb (Cu-mb), and mb isolated following exposure to a 100-fold molar excess of Cu(II), i.e., copper-stabilized (Cu-s-mb), were isolated from *Ms. trichosporium* OB3b as described previously (*8*, *23*). Removal of copper from Cu-s-mb required long-term (approximately 12 h) dialysis against three changes of 5 mM Na_2EDTA in MilliQ water. This dialysis procedure reduced the copper:mb ratio from 1.2 $\pm$ 0.1 to 0.1 $\pm$ 0.02 and for reference purposes was called EDTA-mb. Mb isolated by the procedure of Choi et al. (*8*) contained 0.01 $\pm$ 0.0003 Cu atom per mb. In an attempt to remove the remaining Cu from mb, 10 mL of 10 mM mb was dialyzed for 12 h against three changes of 10 L of 5 mM Na_2EDTA dissolved in MilliQ water. However, following dialysis, the copper:mb molar ratio increased to 0.1 $\pm$ 0.02.

Metal Titration of Mb and EDTA-mb. Metal titration experiments were performed using 50 or 100 μM aqueous solutions of mb or EDTA-mb. Mb and EDTA-mb both buffered the reaction mixtures to pH 6.8. Stock solutions of either $CuSO_4$ or CuCl (100 μM, 1 mM, or 10 mM) were used in metal titrations under both aerobic and anaerobic conditions. For anaerobic titrations, solutions were first degassed using three vacuum−purge cycles with argon and then incubated for 12 h in an anaerobic chamber (Coy Laboratory, Grass Lake, MI) under an atmosphere of 5% hydrogen and 95% argon. In some samples, divided cuvettes (Optiglass Ltd., Hainault, U.K.) were used with copper and mb solutions in different chambers. Cuvettes were sealed and removed from the anaerobic chamber, and their contents were mixed immediately before analysis. In other samples, mb solutions were added to septum cuvettes (Starna cells Inc., Atascadero, CA) in the anaerobic chamber. The cuvettes were sealed before removal from the chamber, and anaerobic solutions of CuCl or $CuSO_4$ were added with gastight syringes. Samples were checked for oxygen contamination using the resazurin-based anaerobic indicator strips (Oxoid Ltd., Basingstoke, Hants, England) in the anaerobic chamber and the indicator strips in a closed anaerobic serum vial.

Spectroscopic Measurements. UV−visible absorption spectroscopy was carried out on either a Cary 50 (Varian Inc.,

Palo Alto, CA) or an Aminco DW2000 (SLM Instruments Inc., Urbana, IL) spectrophotometer.

Fluorescence measurements were recorded on a Cary Eclipse fluorescence spectrophotometer (Varian Inc.). Scan parameters consisted of an excitation slit of 5 nm, an emission slit of 5 nm, and a photomultiplier tube voltage of 600 V. Excitation wavelengths (e.g., 254, 282, 340, and 394 nm) were based on the UV−visible absorption maxima of metal-free mb. $CuSO_4$ and CuCl stock solutions were freshly prepared in MilliQ water (pH 6.8) and kept on ice prior until use. With the exception of time course experiments, all CuCl solutions were mixed between titrations and then incubated for 5 min before spectra were recorded.

Circular dichroism (CD) spectra were recorded between 180 and 585 nm on a JASCO J-710 spectropolarimeter (Jasco Co., Tokyo, Japan) using a 1.0 mm fused quartz cell. $CuSO_4$ and CuCl stock solutions were prepared as described above for fluorescence measurements.

X-ray Photoelectron Spectroscopy (XPS). XPS was performed on a model 5600ci spectrophotometer (Perkin-Elmer Inc., Eden Prairie, MN) as previously described (*46*). The instrument was calibrated at the Au4$f_{7/2}$, Cu2$p_{3/2}$, and Ag3$d_{5/2}$ photopeaks with binding energies of 83.99, 932.66, and 368.27 eV, respectively. A 5 eV flood gun was used to offset charge accumulation. A consistent 800 μm spot size was analyzed using a monochromatized Al Kα ($h\nu = 1486.6$ eV) X-ray source at 300 W and pass energies of 93.9 eV for survey scans and either 58.7 or 5.9 eV for high-resolution scans. The system was operated at a base pressure of 10^{-8}−10^{-9} Torr. An emission angle of 45° was used throughout. Following baseline subtraction, curves were fitted employing combinations of Lorentzian and Gaussian line shapes. Referencing the principal C1*s* photopeak to 284.8 eV accounted for sample charging.

XPS was also performed on a model Phoibos-150 hemispherical analyzer (SPECS Scientific Instruments, Sarasota, FL). The instrument includes a load lock and operates at a routine base pressure of 2.5×10^{-10} Torr. The spectrometer was calibrated on Ag3$d_{5/2}$ and C1*s* from HOPG graphite (Alfa Aesar). Samples were illuminated with Mg Kα X-rays ($h\nu = 1253.6$ eV) from a source operated at 200 W. Spectra for C, N, O, S, and Cu were collected using a consistent spot size of 1.2 mm, normal emission, and a pass energy of 20 eV. The total illumination time with X-rays was ~1.5 h/sample. Using the C1*s* HOPG signal and the Cu^{2+} signal from pure $CuCl_2$, we determined that the N1*s* peak exhibited no appreciable change in peak shape or binding energy; the broad peak was consistently observed at 399.6 eV and served as the reference for all spectra that were collected. Mb was titrated with a 30 mM $CuCl_2$ solution, mixed for 1 min, dripped onto a graphite crystal (HOPG), dried under He, and loaded into vacuum. Spectra were fitted to a Shirley background and peaks with a fixed Gaussian:Lorentzian ratio. Cu2$p_{3/2}$ peaks showed only two states for all samples studied; all Cu peaks had a fwhm of 1.9 eV. S XPS data were fit with two peaks having a fwhm of 1.90 eV. Fitting the data to four peaks to account for spin−orbit splitting of the S2*p* state improved the fit but did not change the binding energy shifts or the conclusions. As with Cu, binding energies were corrected for charging using the N1*s* peak.

Isothermal Titration Calorimetry (ITC). Isothermal titration calorimetry (ITC) was performed on a Microcal (Northampton, MA) VP-ITC microcalorimeter. The instrument was calibrated using the built-in electrical calibration check. All ITC experiments were conducted in water at 25 °C, and solutions were degassed immediately prior to use. Titrant solutions, Cu(II) (800 μM) as $CuSO_4$ in MilliQ H_2O, were added at an interval of 1200 s for injections 1−23 and 300 s for injections 24−60 into the stirred cell containing 100 μM mb, with a stirring rate of 550 rpm. To test for sample stability, the UV−visible absorption spectrum of the sample was monitored at 25 °C. With the exception of the absorption maxima at 340 and 394 nm, the spectrum of mb was stable. The absorption at 340 and 394 nm decreased continuously at a rate of 0.35%/h, or 4.2% during a typical titration series (results not shown). No correction was taken for this possible sample loss. To correct for heats of dilution, control experiments were performed in the absence of mb and were subtracted from the titrations containing mb. Between measurements, the sample cell was washed with the following manufacturers' recommendations. The system was then rinsed three times with 100 μM mb. Data were analyzed using nonlinear least-squares curve fitting in Origin 7.0 (OriginLab Corp., Northampton, MA).

Kinetics of Copper Binding. Kinetic measurements of copper binding were made with a four-syringe Biologic SFM400/S stopped-flow reactor coupled to a MOS 250 spectrophotometer (Bio-Logic Science Instrument SA, Claix, France). This is a four-syringe system with independent drives for each syringe with a minimal dead time of 1.5 ms. Kinetics of binding of copper by mb was monitored at 340 or 394 nm. The reaction mixtures contained 50 μM mb and 25−1000 μM $CuSO_4$. Both reactants were prepared in H_2O, and the final pH following mixing was 6.8.

Kinetic measurements were also carried out using a SX.18MV microvolume stopped-flow reaction analyzer (Applied Photophysics). This is a two-syringe photodiode array system with a minimal dead time of 1.0 ms. Spectral series were measured at 2.0 or 20 °C from 275 to 500 nm using a diode array detector with an integration time of 2.56 ms. Spectra was monitored every 2.6 ms for 500 s. The reaction mixtures, 50 μM mb and 25−250 μM $CuSO_4$ solutions, were prepared in MilliQ H_2O. The mixing chamber had a path length of 1.0 cm, and the monochromator slit width was fixed at 1.0 mm entry and 1.0 mm exit. All samples were protected from ambient light to prevent possible photo-oxidation. Pro-K SVD and global analysis software from Applied Photophysics was used for data analysis. Kinetics of copper binding at fixed wavelengths was derived from the scan series.

Metal, Thiol, and Protein Determinations. Copper and protein determinations were carried out as previously described (*8*). The presence of thiol in mb was determined using the thiol and sulfide quantification kit from Molecular Probes, Inc. (Eugene, OR).

Statistical Analysis. Pearson correlation coefficients and probabilities were determined by bivariant correlation analysis using SPSS 10.1.3 (SPSS Inc., Chicago, IL).

RESULTS

UV−Visible Absorption Spectra of Mb. UV−visible absorption spectra in the 200−800 nm range of mb showed

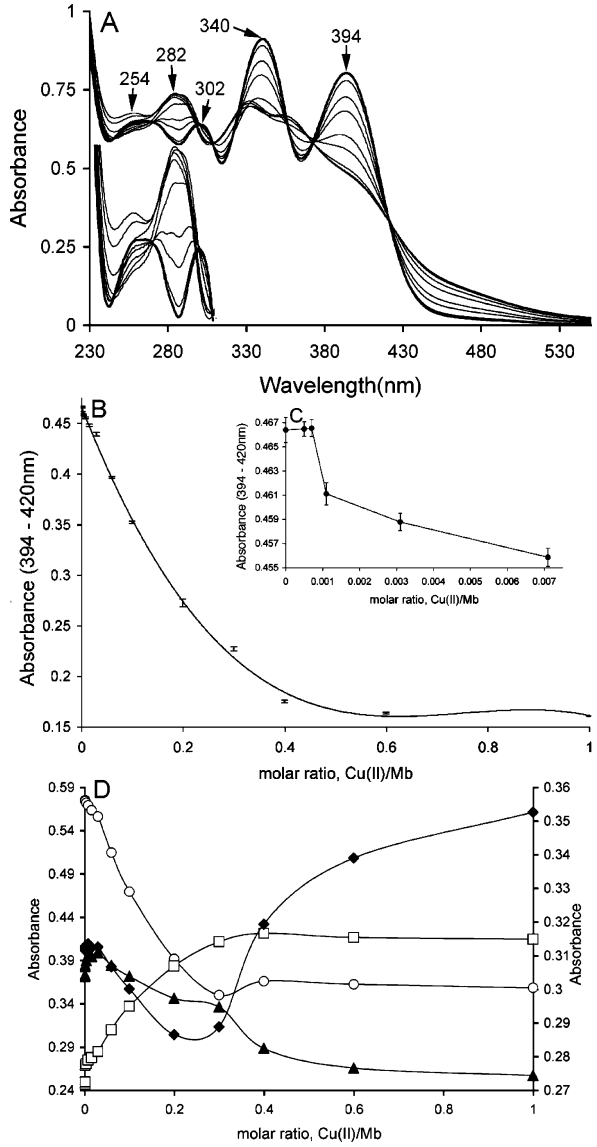

FIGURE 2: (A) UV−visible absorption spectra of mb isolated with a Cu:mb molar ratio of 0.01 and following the addition of 0.003, 0.015, 0.03, 0.06, 0.1, 0.2, 0.3, 0.4, 0.6, and 1.0 Cu(II) atom per mb. (B and C) Absorption changes at 394 nm following Cu(II) additions. (D) Absorption changes at 254 (◆), 282 (□), 302 (▲), and 340 nm (○) following Cu(II) additions. The scale at the right was used for absorption changes at 340 nm, and the scale at the left was used for absorption changes at 254, 282, and 302 nm.

Table 1: Molar Absorption Coefficients (ϵ) of Mb and Cu-mb

metal	wavelengths (nm)	mb ϵ ($mM^{-1}\,cm^{-1}$)	Cu-mb ϵ ($mM^{-1}\,cm^{-1}$)	$\Delta\epsilon$(mb − mb-Cu)
−	394−422	7.14	−	−
−	340−422	8.1		
Cu(II)	394−422	−	2.39	4.75
Cu(II)	340−422		5.16	2.92

absorption maxima at 254, 302, 340, and 394 nm (Figure 2 and Table 1). The spectra were similar to but not identical to the spectra from copper-stabilized mb (Cu-s-mb) samples following dialysis against Na_2EDTA (EDTA-mb), as described by Kim et al. (*23*). The major differences involved the stronger absorption at 340 and 394 nm, and the presence of the small absorption maximum at 302 nm (Figure 2 and Table 1). The selective decreases in the absorption maxima at both 340 and 394 nm in mb have been observed with copper binding (Figure 2), photodegradation (*8*, *23*), and sample storage (see Materials and Methods).

On the basis of the crystal structure of Cu-s-mb (*24*), the absorption maxima at 340 and 394 nm are believed to be associated with HTI and THI, respectively (*23*). If this assumption is correct, the absorption maximum at 394 nm can be tentatively assigned to the THI group associated with the terminal isopropyl ester which has a longer conjugated system (Figure 1). The absorption maximum of HTI would then be assigned to 340 nm. The structure of Cu-s-mb shows copper is coordinated by the N^{ϵ} atom of each imidazole and the S atom of the two-thiocarbonyl groups (Figure 1). Consistent with this chromophore assignment, addition of Cu(II) to mb resulted in a decrease in the absorption maxima at 340 and 394 nm (Figure 2A).

The absorption maxima at 254 nm have been associated with the two Cys moieties of mb (*23*). Interestingly, the absorbance in the 254 nm region decreased until the copper:mb ratios reached 0.25, suggesting further reduction of the Cys population in the sample. At Cu(II):mb ratios of >0.25, the absorbance increases continuously, suggesting oxidation to form cystine consistent with the crystal structure of Cu-s-mb (*24*). The absorption changes near 255 nm have also been reported for Cu(II) complexes with deprotonated nitrogens which give rise to a charge-transfer (CT) absorption in this region (*47*−*49*) and with Cys−S−Cu(I) ligand to metal CT (LMCT) (*50*−*54*). In the case of imidazole (Im), the molar absorption coefficient decreased in the 240−290 nm region with an increase in the molar ratio of copper to imidazole and the absorption maximum was shifted from 278 nm at 0.013 Cu(II) per Im to a shorter wavelength which at 0.3 Cu(II) per Im molar ratio was 254 nm (*47*). Thus, the trend in absorption at 254 nm in Cu(II) titration of mb shows some similarity with copper titration of Im. If the absorption changes at 254 nm during Cu(II) titrations resulted from Cys− or thiocarbonyl−S CT, the results suggest a copper to ligand CT (MLCT) at copper:mb ratios below 0.25 followed by a Cys− or thiocarbonyl−S LMCT at copper:mb ratios above 0.3. The absorbance changes at 254 nm during anaerobic Cu(I) titrations of mb (see below) would be consistent with this S-MLCT/LMCT model.

The absorption maxima at 282 and 302 nm may be associated with phenolic and phenoxide ion forms of tyrosine, respectively (*42*). Consistent with this hypothesis, the increased absorption at 282 nm was associated with the decreased absorption at 302 nm following copper addition (Figure 2D). The phenolic protons of Tyr residues have been shown to ionize under neutral pH conditions when Tyr is the terminal residue or if the peptide contains a Pro residue (*43*, *44*, *55*−*57*). The Tyr in mb is not a terminal residue, nor does it have a Pro residue; however, it does contain a pyrrolidine residue adjacent to the Tyr, which functions structurally as a Pro in the molecule (Figure 1).

Changes in the UV−visible absorption spectra were observed at Cu(II):mb ratios of ≥0.001, or at 50 nM $CuSO_4$ (Figure 2B,C). At lower Cu(II):mb ratios, no spectral changes were observed following corrections for sample dilutions. At copper:mb molar ratios between 0.001 and 0.4, the spectral changes at 340 and 394 nm were proportional to the concentration of Cu(II), but little to no change was observed at Cu:mb molar ratios above 0.6. This latter result was inconsistent with previous Cu(II) binding studies (*8*, *22*)

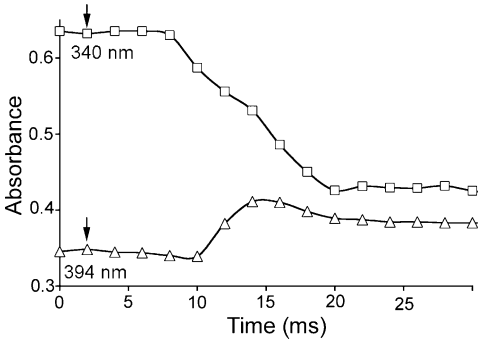

FIGURE 3: Kinetics of binding of Cu(II) by mb. Absorption changes at 340 (□) and 394 nm (△) following the addition of 3 Cu(II) atoms per mb at 20 °C. The arrow indicates the time when the mixing flow stopped.

and metal analysis on samples used in this study. As in previous studies, exposure of mb to a molar excess of Cu(II) over mb resulted in a Cu:mb ratio of 1.2 ± 0.1 (*8*, *15*, *22*). Metal analysis following copper titration experiments showed that at Cu(II):mb molar ratios below 1.1, essentially all of the added copper was bound to mb. In addition, the titration end points were ≤0.85 Cu(II) per mb during isothermal titration calorimetry. Last, the crystal structure of Cu-mb shows one copper atom per mb (*24*). Taken together, the UV−visible absorption results suggest mb binds one Cu per mb and initially binds Cu(II) as a homodimer.

Kinetics of Copper Binding. Binding of Cu(II) by mb from *Ms. trichosporium* OB3b was too fast to measure when saturating concentrations of Cu(II) were used; i.e., the reaction was complete in less than 2.6 ms at 20 or 2 °C (results not shown). In an attempt to reduce the reaction rate, the concentration of Cu(II) was lowered below saturation. Using this approach, spectral changes at 340 nm could be monitored at 20 °C, if the Cu(II):mb ratios were ≤3. Under these conditions, a 6−8 ms lag period was followed by an observed rate constant k_{obsII} of 121 ± 9 s^{-1} (Figure 3). However, even at equimolar concentrations, the reaction rate was too fast to measure at 394 nm with the stopped-flow apparatus that was used, and the k_{obsI} rate was estimated to be >640 s^{-1}. Although the kinetic measurements at 340 nm were obtained at subsaturating Cu(II) concentrations, the results demonstrate the binding of Cu(II) by THI occurred before HTI. Absorption changes were observed at 394 nm under these experimental conditions but were opposite to those observed with copper binding. Specifically, the absorbance at 394 nm increased during binding to the 340 nm chromophore (Figure 3). The reason for this increased absorption at 394 nm was not determined but is consistent with a change in copper coordination from THI alone to a coordination involving both THI and HTI.

Consistent with the spectral properties described here and below, the kinetics of binding of Cu(II) by EDTA-mb differed from that of mb. Using EDTA-mb, the absorption changes at both 394 and 340 nm appeared identical (i.e., k_{obs} > 640 s^{-1}), suggesting initial Cu(II) coordination by both THI and HTI (results not shown).

Fluorescence Spectroscopy. Mb displayed four emission peaks when excited at wavelengths of 254, 282, 340, and 394 nm (Figure 4A). The characteristic emission peak of Tyr at 310 nm was observed following excitation at 282 nm (λ_{ex282}) (*58*, *59*). Excitation at 394 nm (λ_{ex394}) resulted in emissions with maxima at 461, 610, and 675 nm, and excitation at 340 nm (λ_{ex340}) resulted in a broad emission with a maximum at 461 nm. As expected (*60*), excitation at 254 nm (λ_{ex254}) resulted in the Tyr emission peak at 310 nm. Unexpectedly, excitation at 254 nm also resulted in the same emission peaks observed following excitation at 340 nm, i.e., emission at 461 (results not shown). These observations were

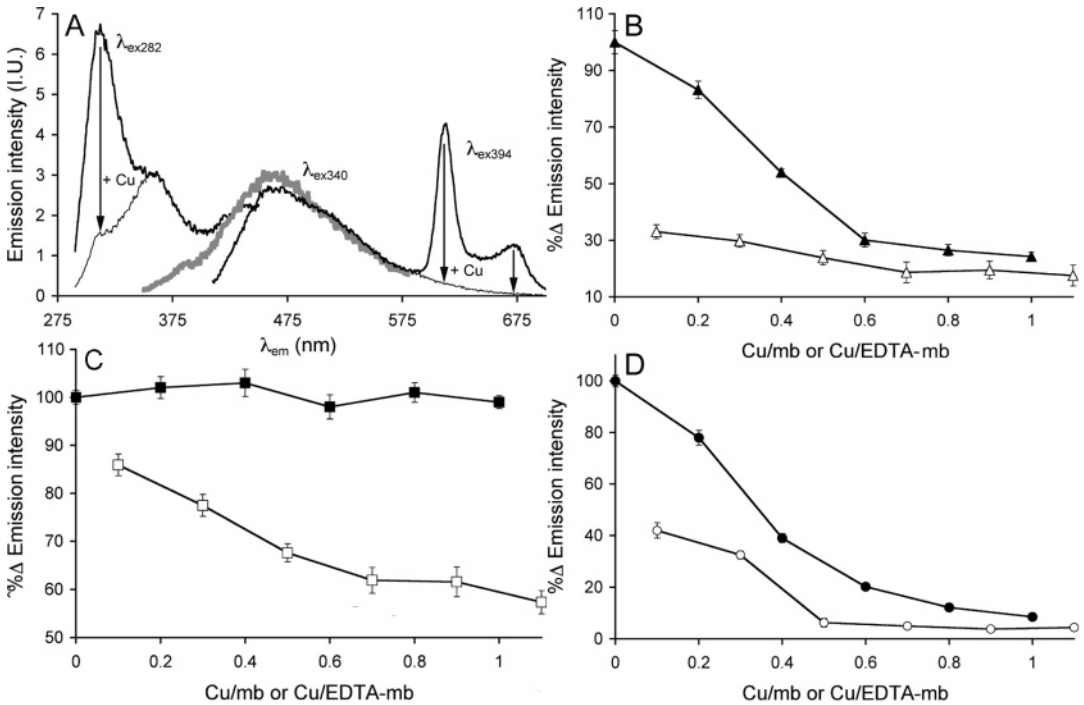

FIGURE 4: (A) Emission spectra of mb in aqueous solution with different excitation wavelengths (λ_{ex} = 282, 340, and 394 nm) at ambient temperature (thick lines). Arrows indicate the direction of spectrum changes upon copper addition, and thin lines show the spectra upon completion of changes. (B−D) Percent emission spectrum changes for mb (▲, ■, and ●) and EDTA-mb (△, □, and ○). Emission spectrum changes were monitored at (B) 310 nm (λ_{ex} = 282 nm), (C) 461 nm (λ_{ex} = 340 nm), and (D) 610 nm (λ_{ex} = 394 nm).

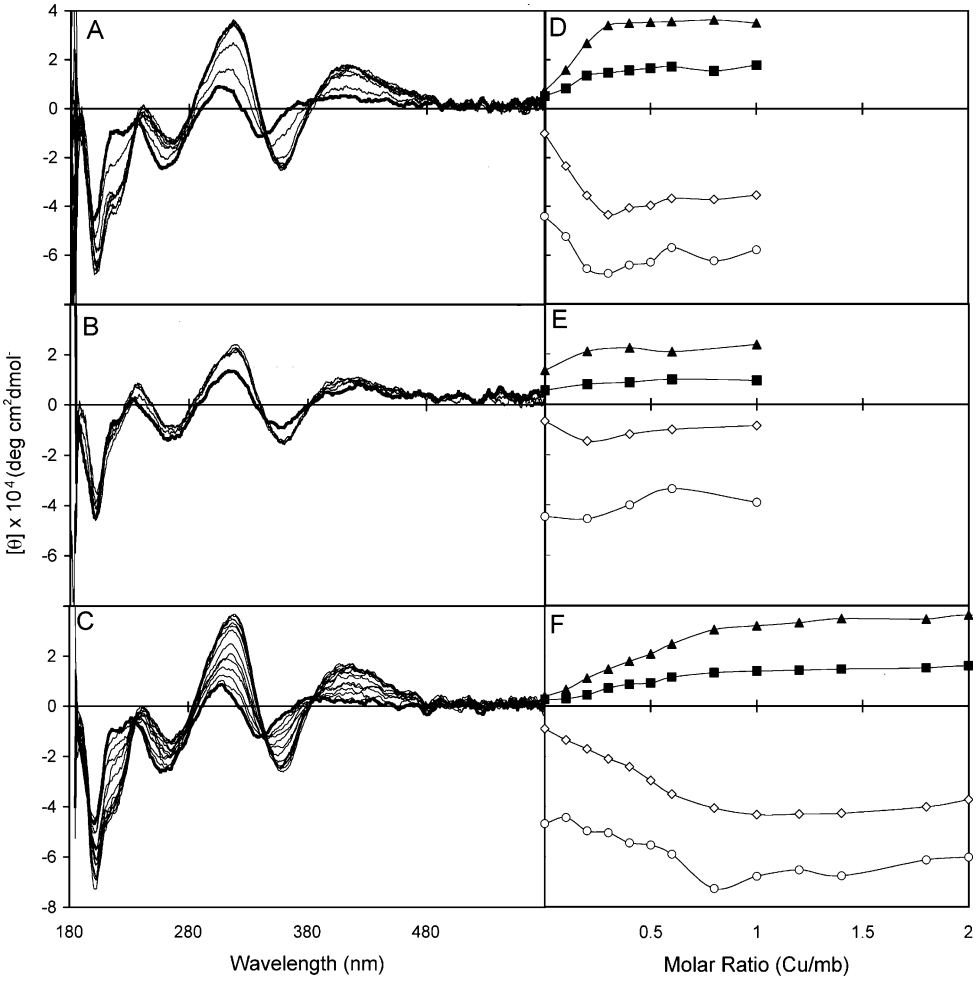

FIGURE 5: Circular dichroism spectra of mb (A and C) and EDTA-mb (B) as isolated (thick line) and following addition of 0.1−1.0 molar equiv of Cu(II) (thin lines) (A and B) or the addition of 0.1−2.0 molar equiv of Cu(I) (thin lines) (C). Panels D−F illustrate the effect of Cu(II) (D and E) or Cu(I) (F) on the CD at 201 (○), 216 (◇), 317 (▲), and 410 nm (■).

different from the emission spectra recently reported by Kim et al. (*23*). The first difference involved the intense emission peak at 280 nm following excitation at 282 nm reported by Kim et al. (*23*). The intense emission at 280 nm appears to be related to the first harmonics following excitation at 280 nm rather than emission from the Tyr, since the emission wavelength was very close to the excitation wavelength and too intense to be emissions from Tyr. Tyr is a comparatively weak fluorophore with a typical Stokes shift of ∼30 nm (*58*−*62*). The intensity of the first harmonics peak would have masked emissions at 310 nm (Figure 4). The second difference was in the emission peaks at 610 and 675 nm following excitation at 394 nm which were not reported by Kim et al. (*23*). In an attempt to determine the reason for the differences reported here and by Kim et al. (*23*), EDTA-mb samples were also examined. The emission spectra following excitations at 282, 340, and 394 nm were similar to the results presented in Figure 4 except the emissions at 310, 461, 610, and 675 nm were only 30−85% of the intensity observed in mb (Figure 4B−D).

The addition of Cu(II) quenched emissions at 310 nm (λ_{ex254} or λ_{ex282}), at 610 nm (λ_{ex254}, λ_{ex282}, λ_{ex340}, or λ_{ex394}), and at 675 nm (λ_{ex394}) (Figure 4), while no changes were observed at the broad emission peak at 461 nm (λ_{ex254}, λ_{ex340}, or λ_{ex394}). This observation also differs from the recent report by Kim et al. (*23*) which showed quenching of the emission at 461 nm by Cu(II). In this case, examination of the spectral properties of EDTA-mb did show the difference resulted from the different sample preparations (Figure 4C). The difference in the degree of quenching of the emissions at 461 nm was probably due to differences in the initial coordination of Cu(II) by mb and EDTA-mb. Quenching of the emission from HTI (i.e., emission at 461 nm) would not be expected to occur if Cu(II) was initially coordinated by THI and possibly Tyr and then reduced to Cu(I) before the coordination to HTI. However, if EDTA-mb was in a conformation similar to that observed in the crystal structure of Cu-s-mb (*24*) (Figure 1) and Cu(II) was initially coordinated by both THI and HTI, quenching of the emissions from HTI (i.e., at 461 nm) should occur along with the quenching of emissions at 610 and 675 nm associated with THI. The results from CD spectra described below suggest this was the case for both mb and EDTA-mb.

Circular Dichroism Spectra. Like many small polypeptides with disulfide bonds, the CD spectrum of mb is of an unordered protein with a strong negative band at 201 nm and weak bands between 211 and 231 nm (Figure 5A) (*63*). The CD spectrum of mb also exhibited weak positive bands at 302 and 364 nm. Following copper addition, the Cu-mb complex showed a decrease in 201 nm along with strong positive bands at 314 nm characteristic of N^-−Cu CT transition and at 406 nm characteristic of phenolate oxygen−

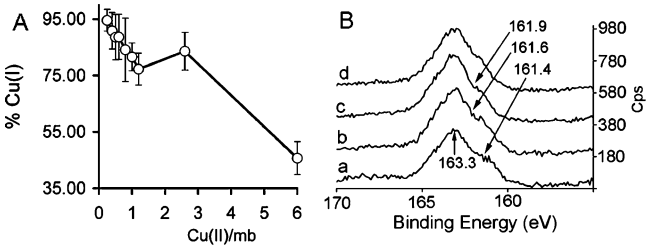

FIGURE 6: (A) Oxidation states of copper at different copper:mb molar ratios as determined by X-ray photoelectric spectroscopy. (B) Sulfur XPS spectra of mb (a) and following the addition of 0.25 (b), 0.5 (c), and 0.75 (d) molar equiv of Cu(II).

Cu CT transition (Figure 5A,D) (*38*, *44*, *56*, *63*, *64*). Alternatively, positive band enhancement near 412 nm (first Cotton effect, THI) and negative band enhancement near 360 nm (second Cotton effect, HTI) can be interpreted as exciton coupled spectra of this two-chromophore system (*65*). In contrast to those of mb, the CD spectra of EDTA-mb were almost identical to those of Cu-mb or to Cu-s-mb, suggesting mb does not return to its native configuration following removal of Cu via dialysis against Na_2EDTA (Figure 5B,E). The largest change in CD spectra following addition of Cu(II) to EDTA-mb was the N^-−Cu CT transition at 314 nm, but even this change showed little correlation to copper concentrations (results not shown). The results suggest there was a comparatively small change in the secondary structure of Cu-mb and Cu-s-mb samples following removal of copper by dialysis against Na_2EDTA.

X-ray Photoelectron Spectroscopy. Previous studies have shown that 60−100% of the copper bound to mb was cuprous copper (*8*, *9*, *15*, *22*−*24*). To address the reason for this variability, several preparations of mb were examined at a variety of Cu(II) concentrations. The results show the percentage of Cu(II) reduced to Cu(I) by mb varied with the copper:mb ratios and decreases from 91 ± 4% at low Cu(II):mb ratios to approximately 75% at equimolar concentrations of Cu(II) and mb (Figure 6A). The <100% reduction of Cu(II) to Cu(I) in reaction mixtures containing low copper concentrations was surprising after examination of higher copper:mb ratios (Figure 6A). The source of the reductants in mb has not been determined. As described in UV−Visible Absorption Spectra of Mb, the spectral changes in the 250 nm range following Cu(II) additions may represent changes in the oxidation state of Cys-S. High-resolution XPS spectra (pass energy of 10 eV) for sulfur from mb were used to examine this possibility (Figure 6B). Fitting the data for metal-free mb revealed two S states: a large peak at 163.3 eV representing 69% of the sulfur signal and a smaller peak at 161.4 eV (Figure 6B). The major peak at 163.3 mV was assigned to Cys and Met S based on the reported binding energies of 163.6 eV for both Cys (thiol) and Met S (*66*−*68*). Formation of a disulfide bridge between two Cys shifts the S binding energy up by approximately 0.5 eV (*67*). The addition of Cu(II) to mb did not alter the XPS signal at 163.3 eV, and the absence of a new state at energies above 163.3 eV suggests either the expected disulfide signal was below our detection limits or the oxidation state of S on Cys did not change. Attempts to quantify the thiols of mb at the beginning and end of the titration by the method of Singh et al. (*69*) failed, suggesting the sulfhydryl groups of the two Cys were oxidized in the initial and final sample. These results suggest that the peak at 163.3 eV arises from Met S and Cys as a disulfide.

The smaller peak at 161.4 eV was attributed to the thiocarbonyl S (*66*−*68*). Studies of thiourea report a S binding energy of 162 eV, which becomes 0.5−0.7 eV higher upon binding to Cu. In contrast to thiourea, the thiocarbonyl groups of mb are bound to a hydroxyimidazole group, which extends the local conjugation. The observed binding energy for mb thiocarbonyl S at 161.4 eV reflects this stronger conjugation. Binding of mb to Cu shifts the observed binding energy up to 161.9 eV, consistent with results for binding of thiourea-based model compounds to Cu (*66*, *67*). The completed binding energy shift of the thiocarbonyl S states at a copper:mb ratio of 0.5 Cu per mb indicates that mb initially binds Cu as a dimer.

Thermodynamic Properties of Cu(II) Binding by Mb. Initial isothermal titration calorimetry (ITC) experiments for Cu(II) binding by mb from *Ms. trichosporium* OB3b showed a difference in thermodynamic properties at copper:mb ratios of 0.2 and 0.45 with a titration end point at 0.85 Cu(II) per mb (Figure 7 and Table 2). When the titration data in this copper concentration range were analyzed by nonlinear least-squares curve fitting in Origin 7.0, they fit a two-site model better than a one-binding site model (Table 2). A third high-affinity binding constant was also observed at Cu:mb ratios below 0.2 (Figure 7E,F and Table 2). However, attempts to determine the binding constant at low copper:mb ratios proved to be difficult. Decreasing titrant concentrations resulted in an unstable baseline due to the small energy change, and increasing mb concentrations above 1.8 mM resulted in sample precipitation following copper additions. Measurements between 0.07 and 0.2 Cu per mb provided reasonable results with excellent curve fits with a K of $3.25 \times 10^{34} \pm 3.0 \times 10^{11}$ and a $\Delta G°$ of −47.16 kcal/mol. The high K below 0.2 Cu per mb was comparable to the binding constants observed for Fe(III) binding by peptide siderophores (*33*, *34*) but orders of magnitude higher than that expected for copper binding given the structure (*40*, *45*, *48*, *57*, *70*−*72*) even if mb initially binds as a multimer (*73*, *74*). Given the few titration points, we feel it prudent to estimate the initial K of mb to be $>8 \times 10^{18}$. This binding constant at low Cu:mb ratios was based on the greater affinity of mb over Na_2EDTA which has a log K_{EDTA} of 18.8 at pH 7.0 for Cu(II) (*75*) (see Materials and Methods). The complex pattern of Cu(II) binding was also consistent with spectral (UV−visible, fluorescence, CD, and EPR) and gel filtration data (*8*, *22*), suggesting a series of subunit interactions and/or conformational changes during Cu(II) binding and reduction.

ITC was also used to determine if the spectral changes that occur during dialysis against Na_2EDTA to remove copper from Cu-s-mb samples by dialysis against Na_2EDTA (EDTA-mb) affected the copper binding properties of the molecule. As shown in Table 2, the initial high-affinity copper properties were lost, and the remaining copper binding constants decreased by 1−1.5 orders of magnitude. Using the isolation procedure described by Choi et al. (*8*), the Cu:mb, Cu:Cu-s-mb, and Cu:EDTA-mb molar ratios were 0.01, 1.2, and 0.1, respectively. Thus, the initial Cu concentration in EDTA-mb samples could account for the loss of the first high-affinity binding constant but not for the lower binding constants at copper ratios above 0.1 copper per mb.

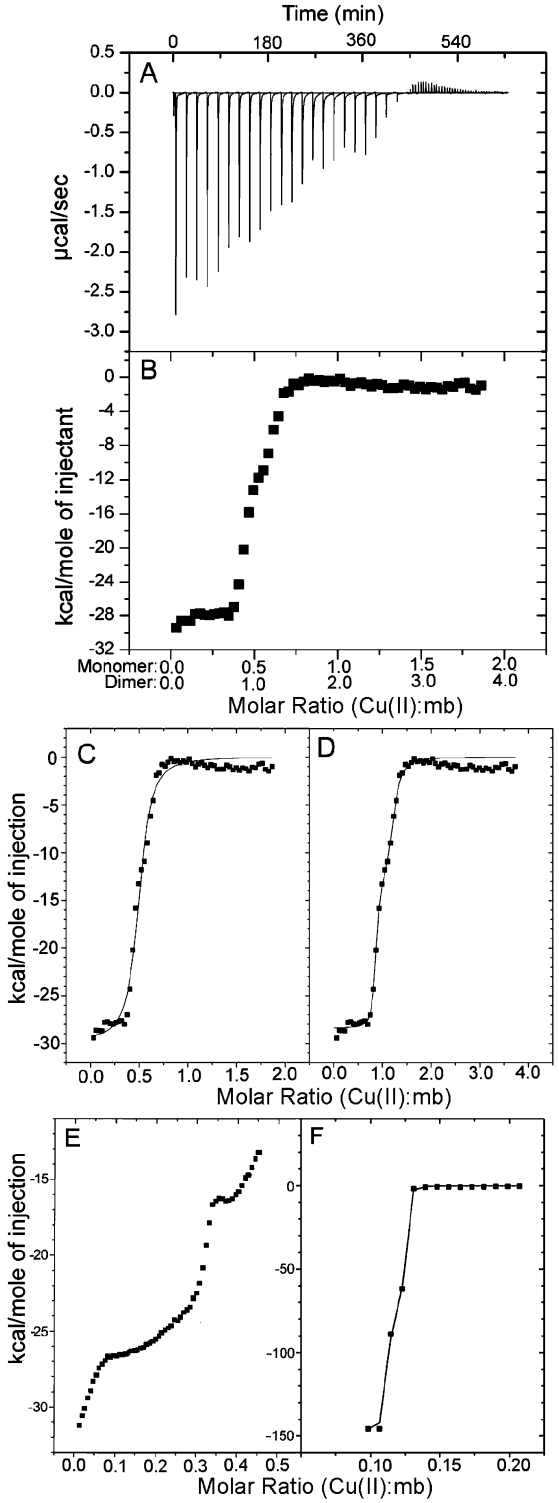

FIGURE 7: Thermogram (A) and binding isotherm (B) showing additions of $CuSO_4$ (60 separate 5 μL injections from a 800 μM $CuSO_4$ solution) to 100 μM mb (cell) in water at 25 °C. Panel C shows a binding isotherm showing the curve fitting for a one-site binding algorithm, and panel D shows a binding isotherm showing the curve fitting for a two-site binding algorithm. Panels E and F show binding isotherms showing the curve fitting for a two-site binding algorithm at low Cu(II) concentrations. Copper and mb concentrations in panels E and F were increased to 1.6 mM and 800 μM, respectively.

Solubilization and Binding of Cu(I) by Mb and EDTA-mb. In addition to Cu(II), mb will also bind and solubilize Cu(I) under both aerobic and anaerobic conditions (Figures 8 and 9). The UV−visible absorption (Figures 8 and 9), fluorescence (results not shown), and CD (Figure 5C,F) spectral changes observed during Cu(I) titrations where similar to those for Cu(II) titrations, except the changes in the titration trends occurred at approximately 1 Cu(I) per mb suggesting mb bound Cu(I) as a monomer (Figure 8). Also in contrast to Cu(II) (Figure 2), a Cu(I):mb ratio of 1.5−2.0 was required to saturate the UV−visible absorption changes (Figure 8B). The Cu(I):mb ratios above 1 suggest mb may have a weak secondary copper-binding site. The spectral changes at 254 nm may represent this secondary binding site (Figure 8) and involve the two Cys moieties or may represent a change from Cys− or thiocarbonyl−S MLCT to Cys− or thiocarbonyl−S LMCT.

The kinetics of Cu(I) binding at 394 nm following addition of Cu(I) to mb was also similar to that of Cu(II); i.e., $k_{obsI} > 640\ s^{-1}$. However, the kinetics of binding to HTI (i.e., absorption changes at 340 nm) was significantly slower ($k_{obsII} = 8.27 \pm 0.16\ s^{-1}$). The kinetics of Cu(I) binding by mb was similar under aerobic and anaerobic conditions, suggesting mb bound Cu(I) before dismutation of Cu(I) to Cu(II) occurred (Figure 9). Since the kinetic differences in k_{obsII} between Cu(II) and Cu(I) were large, the addition of Cu(II) before coordination of Cu(I) to HTI was used to determine if Cu(II) could displace mb from the surface of insoluble CuCl (Figure 9B). The addition of Cu(II) after completion of the spectral changes at 394 nm but before completion of the spectral changes at 340 nm resulted in a small increase in absorption at both 340 and 394 nm but did not alter the kinetics of Cu(I) binding. Simultaneous addition of both Cu(II) and Cu(I) also followed the slower k_{obsII} Cu(I) kinetic trace at 340 nm, suggesting mb has a higher affinity for Cu(I) or that the kinetics of binding to Cu(I) as a monomer was faster than binding to Cu(II) as a dimer. Because of solubility problems with Cu(I) solutions, the thermodynamics of Cu(I) binding by mb was not determined.

As expected, Cu(I) did not quench luminescence under anaerobic conditions from either mb or EDTA-mb. The UV−visible absorption spectral changes following Cu(I) additions under anaerobic conditions were identical to those aerobic conditions demonstrating binding. Thus, the oxidation state of copper had no effect on the UV−visible absorption spectra of mb (Figure 8B,C) which was consistent with previous EPR studies (*8*). Luminescence was quenched in Cu-mb samples following Cu(I) binding under aerobic conditions (Figure 9C). The luminescence quenched by Cu(I) following the addition of air can be explained by the dismutation of aqueous Cu(I) to Cu(II) in the presence of oxygen. When Cu(II) was added to Cu(I)-mb under anaerobic conditions, luminescence was also quenched at emission peaks of 310 and 610 nm within 30 s, but not at 461 nm (Figure 9C). The results shown in Figure 9C suggest Cu(I)-mb undergoes a second Cu(II) binding sequence, which would involve coordination of Cu(II) to THI and possibly Tyr, followed by reduction to Cu(I) before coordination by HTI. XPS data described above showed mb can reduce more than 2 Cu(II) atoms per mb (Figure 8). Whether HTI remains coordinated to the first Cu(I) through this proposed second binding series and whether Cu(I) remains associated with mb have not been determined.

Table 2: Thermodynamic Parameters for Binding of Cu(II) to Mb at pH 6.8[a]

parameter	mb monomer model	mb_2 dimer model	mb_2-EDTA-treated dimer model
N_1 (Cu mb^{-1})	0.495 ± 0.005	0.11 ± 0002	−
K_1 (M^{-1})	$(1.12 \pm 0.16) \times 10^6$	$>8 \times 10^{18}$	−
ΔH_1 (kcal mol^{-1})	-29.8 ± 0.41	ca. −146	−
ΔS_1 (cal mol^{-1} deg^{-1})	−72.2	ca. −331	−
ΔG_1 (kcal mol^{-1})	−8.25	ca. −47	−
N_2 (Cu mb^{-1})	−	0.14 ± 0.013	0.14 ± 0.003
K_2 (M^{-1})	−	$(2.6 \pm 0.47) \times 10^8$	$(2.3 \pm 0.41) \times 10^7$
ΔH_2 (kcal mol^{-1})	−	-28.04 ± 0.11	-29.3 ± 0.38
ΔS_2 (cal mol^{-1} deg^{-1})	−	−55.6	−65.8
ΔG_2 (kcal mol^{-1})	−	−11.46	−9.7
N_3 (Cu mb^{-1})	−	0.37 ± 0.02	0.27 ± 0.017
K_3 (M^{-1})	−	$(1.40 \pm 0.21) \times 10^6$	$(6.7 \pm 0.11) \times 10^4$
ΔH_3 (kcal mol^{-1})	−	-12.83 ± 0.49	-11.4 ± 0.79
ΔS_3 (cal mol^{-1} deg^{-1})	−	−14.9	−16.3
ΔG_3 (kcal mol^{-1})	−	−8.38	−6.58
χ^2	1.01×10^6	6.47×10^4	2.78×10^5

[a] The monomer and dimer model was based on best fits using a one- or two-binding site model.

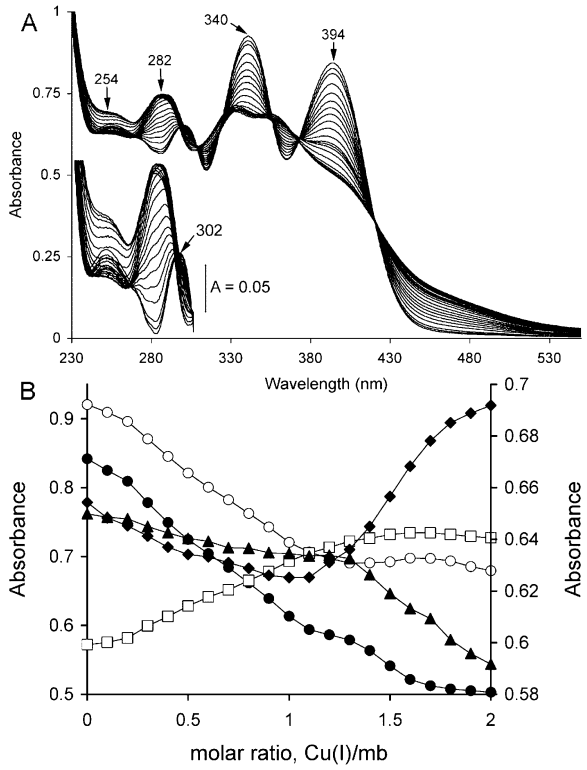

FIGURE 8: (A) UV−visible absorption spectra of mb following the addition of 0−2.0 Cu(I) atoms per mb in increments of 0.1 molar equiv. (B) Absorption changes at 254 (◆), 282 (□), 302 (◆), 340 (○), and 394 nm (●) following Cu(I) additions. The scale at the left was used for absorption changes at 282, 340, and 394 nm, and the scale at the right was used for absorption changes at 254 and 302 nm.

DISCUSSION

The isolation procedure for mb described by Choi et al. (*8*) provides for the first time mb samples suitable for metal binding studies. Kim et al. (*23*, *24*) have recently reported the isolation of Cu-s-mb. Samples isolated following copper stabilization are much more resistant to sample breakdown, are less photolabile, and function well in the stimulation of pMMO activity (*8*, *23*). Cu-s-mb also results in a homogeneous sample (*8*) that probably aided in the crystallization of the molecule for structural characterization (*24*). However, removal of the copper from Cu-s-mb following exposure to high copper concentrations results in samples with altered spectral (UV−visible absorption, CD, and fluorescence) properties and lower binding constants when compared to those of mb isolated by the procedures described by Choi et al. (*8*). The Na_2EDTA treatment described by Kim et al. (*23*) was successful in the removal of approximately 90% of the copper associated with Cu-s-mb. However, the results presented here suggest the molecule does not return to its original structure. In this study, EDTA-mb provided an interesting comparison to mb, since this sample appears to maintain the Cu-s-mb structure and initially binds Cu(II) and Cu(I) via the THI and HTI groups as predicted from the crystal structure of Cu(I)-mb (*23*).

With respect to the mechanism of copper binding, the kinetic, spectral, and thermodynamic studies shown here indicate Cu(II) binding was dependent on the Cu(II):mb ratio and may involve inter- and intramolecular binding similar to that observed with prion proteins (*76*−*78*). Formation of distinct Cu−thiolate clusters has also been observed in mammalian metallothioneins at different Cu:metallothionein ratios (*51*, *52*). On the basis of the structure of mb, THI has a longer conjugated system and is probably the group responsible for the absorption maxima at 394 nm. If this prediction is true, our working model for binding of Cu(II) involves the following steps (Figure 10). Mb initially bound Cu(II) as a dimer (Figure 10, I), with Cu(II) coordinated to THI and possibly Tyr. This proposed initial coordination was based by the lag time and slower kinetic properties when the reaction was monitored at 340 nm. Binding as a dimer was based on the saturation of spectral (UV−visible, CD, and fluorescence) properties, and the completed binding energy shift of the thiocarbonyl S state changes at approximately 0.5 Cu(II) per mb. Previous gel filtration chromatography of mb at different Cu(II):mb ratios also suggests dimer formation (*8*). In addition to the THI groups, spectral changes also suggested Tyr was involved in the initial binding of copper by mb. Time course fluorescence changes associated with Tyr following Cu(I) addition were kinetically identical to those of THI, suggesting the quenching of the Tyr signal was coupled with THI (results not shown).

The reduction step (Figure 10, II) in the binding process could not be determined directly. However, the absence of quenching of the 461 nm emission following excitation at

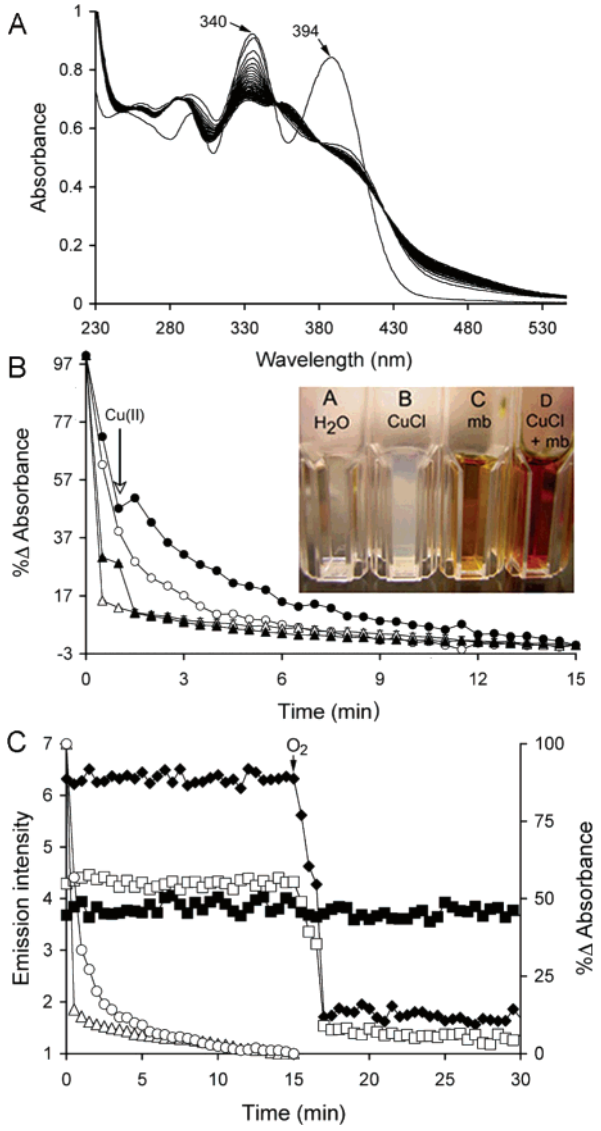

FIGURE 9: (A) UV−visible absorption spectra of mb from *Ms. trichosporium* OB3b spectra taken every 30 s following the addition of CuCl. (B) Percent absorption change over time at 340 (○) and 394 nm (◇) and at 340 (●) and 394 nm (◆) in the presence of Cu(II), arrow marks the time of Cu(II) addition. Inset, solubilization of CuCl by mb, A, H_2O blank; B, 100 μM CuCl to 100 μM mb; C, 100 μM mb; and D, 6 min after addition of 100 μM CuCl to 100 μM mb. (C) UV−visible absorption changes at 340 (○) and 394 nm (△) and emission intensity changes at 310 nm (λ_{ex} = 282 nm) (◆), 461 nm (λ_{ex} = 340 nm) (■), and 610 nm (λ_{ex} = 394 nm) (□) following addition of a 3-fold molar excess of CuCl under anaerobic conditions. The arrow indicates the time of exposure to air (O_2).

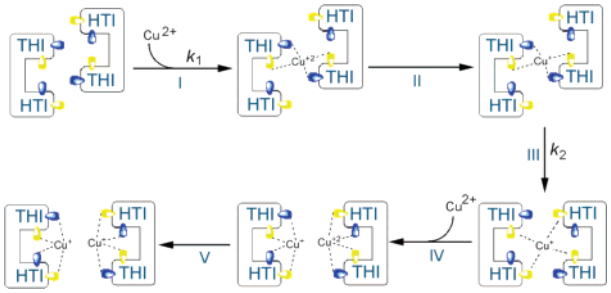

FIGURE 10: Model for Cu(II) binding by mb. Abbreviations: yellow symbol, thiocarbonyl group; blue symbol, imidazole N^{ϵ} atom.

340 nm suggests the copper was reduced before coordination to HTI. Emission at 461 nm was quenched in EDTA-mb samples demonstrating emissions from HTI can be quenched if exposed to Cu(II), but not by Cu(I) as shown in the fluorescence spectra of Cu(I) titration under anaerobic conditions. The source of the reductant has not been determined. Like Kim et al. (*23*), we initially believed the Cys thiols were the source reductants in this reaction. However, the decreased absorption at 254 nm at Cu(II):mb ratios of ≤0.25 was inconsistent with Cys thiols being the electron source. In addition, attempts to measure Cys thiols chemically or via XPS were unsuccessful. The changes at 254 nm appeared to be more consistent with either a CT between Cu and imidazole nitrogen or a Cys− or thiocarbonyl−S CT. Emission at 461 nm following excitation at 254 nm also suggests absorption at 254 nm is associated with HTI.

The third step (Figure 10, III) in the reaction involves the change in coordination from the thiocarbonyl and N^{ϵ} of THI to four thiocarbonyl sulfurs from two THI and two HTI groups. The proposed change in copper coordination from two THI groups to two THI groups and two HTI groups is based on the lag period between completion of binding at THI and initial coordination to HTI, and the increased absorption by THI during coordination to HTI. This change in copper coordination was consistent with previous EPR studies which showed more than one cupric site at low Cu(II):mb ratios (*8*). XPS data also suggest all four binding sites are through thiocarbonyl sulfur at 0.5 Cu per mb.

The addition of the second Cu(II) to the mb dimer (Figure 10, IV and V) results in the change in coordination from all thiocarbonyl S to a dual N and S coordination similar to that shown in the crystal structure of Cu-s-mb (*24*). The change in the Cu(II) binding constant and the increased nitrogen coordination at Cu(II):mb ratios above 0.5 (*8*) were consistent with this change in copper coordination.

The results presented in this study suggest mb is a dynamic molecule in solution. Monomer, dimer, and potential oligomers of mb have been observed by gel filtration chromatography (*8*, *22*). In the absence of copper, mb migrates into several fractions via reverse phase chromatography, indicating a mixed population (*8*, *23*). Analysis of each fraction by gel filtration or reverse phase chromatography generated chromatographs similar to the original (*8*, *22*−*24*), suggesting mb exists in solution as a mixture of monomer and oligoimers or the molecule exists in several different conformations. Homogeneous mb samples can be generated via incubation of the samples in the presence of excess concentrations of copper or storage on ice for 2−3 days (*8*, *23*, *24*). These treatments alter the spectral and thermodynamic properties of the sample but do not alter the stimulatory effects of Cu-mb on methane oxidation by the pMMO (*8*). Whether a dimer or mixed population theory is used, the results presented here indicate mb is a dynamic molecule in solution and does show properties consistent with a chalkophore.

ACKNOWLEDGMENT

We thank V. Frasca at Microcal for assistance in modeling of the ITC results. We also thank to Drs. J. Petrich (Iowa State University) and J. Applequest (Iowa State University) for helpful discussions.

REFERENCES

1. Anthony, C. (1982) *The Biochemistry of Methylotrophs*, Academic Press, London.
2. Dalton, H., Prior, S. D., Leak, D. J., and Stanley, S. H. (1984) Regulation and control of methane monooxygenase, in *Microbial Growth on C_1 Compounds* (Crawford, R. L., and Hanson, R. S., Eds.) pp 75−82, American Society for Microbiology, Washington, DC.
3. DiSpirito, A. A., Gulledge, J., Schiemke, A. K., Murrell, J. C., and Lidstrom, M. E. (1992) Trichloroethylene oxidation by the membrane-associated methane monooxygenase in type I, type II, and type X methanotrophs, *Biodegradation 2*, 151−164.
4. Hanson, R. L., and Hanson, T. E. (1996) Methanotrophic bacteria, *Microbiol. Rev. 60*, 439−471.
5. Lontoh, S., DiSpirito, A. A., and Semrau, J. D. (1999) Dichloromethane and trichloroethylene inhibition of methane oxidation by the membrane-associated methane monooxygenase of *Methylosinus trichosporium* OB3b, *Arch. Microbiol. 173*, 29−34.
6. Basu, P., Katterle, B., Anderson, K. A., and Dalton, H. (2002) The membrane-associated form of methane monooxygenase from *Methylococcus capsulatus* (Bath) is a copper/iron protein, *Biochem. J. 369*, 417−427.
7. Chan, S. I., Chen, K. H.-C., Yu, S. S.-F., Chen, C.-L., and Kuo, S. S.-J. (2004) Tword delineating the structure and function of the particulate methane monooxygenase from methanotrophic bacteria, *Biochemistry 43*, 4421−4430.
8. Choi, D.-W., Antholine, W. A., Do, Y. S., Semrau, J. D., Kisting, C. J., Kunz, R. C., Campbell, D., Rao, V., Hartsel, S. C., and DiSpirito, A. A. (2005) Effect of methanobactin on methane oxidation by the membrane-associated methane monooxygenase in *Methylococcus capsulatus* Bath, *Microbiology 151*, 3417−3426.
9. Choi, D.-W., Kunz, R. C., Boyd, E. S., Semrau, J. D., Antholine, W. A., Han, J.-I., Zahn, J. A., Boyd, J. M., de la Mora, A. M., and DiSpirito, A. A. (2003) The membrane-associated methane monooxygenase (pMMO) and pMMO-NADH:quinone oxidoreductase from *Methylococcus capsulatus* Bath, *J. Bacteriol. 185*, 5755−5764.
10. DiSpirito, A. A., Kunz, R. C., Choi, D. W., and Zahn, J. A. (2004) Electron flow during methane oxidation in methanotrophs, in *Respiration in Archaea and Bacteria* (Zannoni, D., Ed.) pp 141−169, Kluwer Scientific, Dordrecht, The Netherlands.
11. Morton, J. D., Hayes, K. F., and Semrau, J. D. (2000) Bioavailability of chelated and soil-absorbed copper to *Methylosinus trichosporium* OB3b, *Environ. Sci. Technol. 34*, 4917−4922.
12. Nguyen, A.-N., Schiemke, A. K., Jacobs, S. J., Hales, B. J., Lidstrom, M. E., and Chan, S. I. (1994) The nature of the copper ions in the membranes containing the particulate methane monooxygenase from *Methylococcus capsulatus* (Bath), *J. Biol. Chem. 269*, 14995−15005.
13. Nguyen, H.-H., Elliott, S. J., Yip, J. H.-K., and Chan, S. I. (1998) The particulate methane monooxygenase from *Methylococcus capsulatus* (Bath) is a novel copper-containing three-subunit enzyme, *J. Biol. Chem. 273*, 7957−7966.
14. Takeguchi, M., Miyakawa, K., and Okura, I. (1998) Purification and properties of particulate methane monooxygenase from *Methylosinus trichosporium* OB3b, *J. Mol. Catal. 132*, 145−153.
15. Zahn, J. A., and DiSpirito, A. A. (1996) Membrane associated methane monooxygenase from *Methylococcus capsulatus* (Bath), *J. Bacteriol. 178*, 1018−1029.
16. Han, J.-I., and Semrau, J. D. (2001) Quantification of the expression of *pmoA* in methanotrophs using RT-PCR, *Proc. Am. Chem. Soc.* Abstract no. 221.
17. Han, J.-I., and Semrau, J. D. (2004) Quantification of gene expression in methanotrophs by competitive reverse transcription-polymerase chain reaction, *Environ. Microbiol. 6*, 388−399.
18. Lontoh, S., and Semrau, J. D. (1998) Methane and trichloroethylene degradation by *Methylosinus trichosporium* expressing particulate methane monooxygenase, *Appl. Environ. Microbiol. 64*, 1106−1114.
19. Murrell, J. C., McDonald, I. R., and Gilbert, B. (2000) Regulation of expression of methane monooxygenases by copper ions, *Trends Microbiol. 8*, 221−225.
20. Prior, S. D., and Dalton, H. (1985) Copper stress underlies the fundamental change in intracellular location of methane monooxygenase in methane oxidizing organisms: Studies in batch and continuous culture, *J. Gen. Microbiol. 131*, 155−163.
21. Stanley, S. H., Prior, S. D., Leak, D. J., and Dalton, H. (1983) Copper stress underlies the fundamental change in intracellular location of methane monooxygenase in methane-oxidizing organisms: Studies in batch and continuous cultures, *Biotechnol. Lett. 5*, 487−492.
22. DiSpirito, A. A., Zahn, J. A., Graham, D. W., Kim, H. J., Larive, C. K., Derrick, T. S., Cox, C. D., and Taylor, A. (1998) Copper-binding compounds from *Methylosinus trichosporium* OB3b, *J. Bacteriol. 180*, 3606−3616.
23. Kim, H. J., Galeva, N., Larive, C. K., Alterman, M., and Graham, D. W. (2005) Purification and physical-chemical properties of methanobactin: A chalkophore from *Methylosinus trichosporium* OB3b, *Biochemistry 44*, 5140−5148.
24. Kim, H. J., Graham, D. W., DiSpirito, A. A., Alterman, M., Galeva, N., Asunskis, D., Sherwood, P., and Larive, C. K. (2004) Methanobactin, a copper-acquisition compound in methane-oxidizing bacteria, *Science 305*, 1612−1615.
25. Tellez, C. M., Gaus, K. P., Graham, D. W., Arnold, R. G., and Guzman, R. Z. (1998) Isolation of copper biochelates from *Methylosinus trichosporium* OB3b, *Appl. Environ. Microbiol. 64*, 1115−1122.
26. Phelps, P. A., Agarwal, G. E., Speitel, G. E. J., and Georgiou, G. (1992) *Methylosinus trichosporium* OB3b mutants having constitutive expression of soluble methane monooxygenase in the presence of high levels of copper, *Appl. Environ. Microbiol. 58*, 3701−3708.
27. Bielli, P., and Calabrese, L. (2002) Structure to function relationships in ceruloplasmin: A 'moonlighting' protein, *Cell. Mol. Life Sci. 59*, 1413−1427.
28. Jeffery, C. J. (1999) Moonlighting Proteins, *Trends Biochem. Sci. 24*, 8−11.
29. Jeffery, C. J. (2003) Moonlighting proteins: Old proteins learning new tricks, *Trends Genet. 19*, 415−417.
30. Jeffery, C. J. (2004) Molecular mechanisms for multitasking: Recent crystal structures of moonlighting proteins, *Curr. Opin. Struct. Biol. 14*, 663−668.
31. Moor, B. D. (2004) Bifunctional and moonlighting enzymes: Lighting the way to regulatory control, *Trends Plant Sci. 9*, 221−228.
32. Tompa, P., Szasz, C., and Buday, L. (2005) Structural disorder throws a new light on moonlighting, *Trends Biochem. Sci. 30*, 484−489.
33. Neilands, J. B. (1995) Siderophores: Structure and function of microbial iron transport compounds, *J. Biol. Chem. 270*, 26723−26726.
34. Nielands, J. B. (1983) Siderophores, *Adv. Inorg. Biochem. 5*, 138−166.
35. Bonomo, R. P., Cali, R., Cucinotta, V., Impellizzeri, G., and Rizzarelli, E. (1986) Copper(II) complexes of diastereoisomeric dipeptides in aqueous solutions. Effects of side-chain groups on the thermodynamic sterioselectivity, *Inorg. Chem. 25*, 1641−1646.
36. Letter, J. E., and Bauman, J. E. J. (1970) A thermodynamic study of the complexation and coordinated ligand deprotonation reactions for a series of tyrosine isomer with copper(II), *J. Am. Chem. Soc. 92*, 443−447.
37. Livera, C., Pettit, L. D., Bataille, M., Bal, W., and Kozlowskim, H. (1988) Copper(II) complexes with some tetrapeptides containing the 'break-point' prolyl residue in the third position, *J. Chem. Soc., Dalton Trans.*, 1357−1360.
38. Osz, K., Boka, B., Vamagy, K., Sovago, I., Kurtan, T., and Antus, S. (2002) The application of circular dichroism spectroscopy for the determination of metal ion speciation and coordination modes of peptide complexes, *Polyhedron 21*, 2149−2159.
39. Pecci, L., Molntefoschi, G., Musci, G., and Cavallini, D. (1997) Novel findings on the copper catalyzed oxidation of cysteine, *Amino Acids 13*, 355−367.
40. Pettit, L. D., Steel, I., Formica-Kozlowski, G., Tatarowski, T., and Bataille, M. (1985) The L-proline residue as a 'break-point' in metal-peptide systems, *J. Chem. Soc., Dalton Trans.*, 535−539.
41. Rigo, A., Corazza, A., de Paolo, M. L., Rossetto, M., Ugolini, R., and Scarpa, M. (2004) Interaction of copper with cysteine: Stability of cuprous complexes and catalytic role of cupric ions in anaerobic thiol oxidation, *J. Inorg. Biochem. 98*, 1495−1501.
42. Greenstein, J. P., and Winitz, M. (1961) *Chemistry of the Amino Acids*, Vol. 2, John Wiley & Sons, Inc., New York.
43. Hefford, R. J. W., and Pettit, L. D. (1981) Potentiometric and spectrophotometric study of the co-ordination compounds formed between copper(II) and dipeptides containing tyrosine, *J. Chem. Soc., Dalton Trans.*, 1331−1335.
44. Kozlowska, H., Benzer, M., Pettit, L. D., and Hecquet, B. (1983) Coordination abilities of tetrapeptides containing proline and

tyrosine-a spectrometric and potentiometric study, *J. Inorg. Biochem. 18*, 231−240.
45. Pettit, L. D., Steel, I., Kowalik, T., Kozlowski, H., and Bataille, M. (1985) Specific binding of the tyrosine residue in copper(II) complexes of tyr-pro-gly-tyr and tyr-gly-pro-tyr, *J. Chem. Soc., Dalton Trans.*, 1201−1205.
46. Neil, A. L., Techkarinjanarukm, S., Dohnalkova, A., McCready, D., Peyton, B. M., and Geesey, G. G. (2001) Iron sulfides and sulfur species produced at hematite surfaces in the presence of sulfate-reducing bacteria, *Goechim. Cosmochim. Acta 65*, 223−235.
47. Edsall, J. T., Felsenfeld, G., Goodman, D. S., and Gurd, F. R. N. (1954) The association of imidazole with the ions of zinc and cupric copper, *J. Am. Chem. Soc. 76*, 3054−3061.
48. Sigel, H., and Martin, R. B. (1982) Coordinating properties of the amide bond. Stability and structure of metal ion complexes of peptides and related ligands, *Chem. Rev. 82*, 385−426.
49. Tsangaris, J. M., Chang, J. W., and Martin, R. B. (1969) Ultraviolet circular dichroism of cupric and nickel complexes of amino acids and peptides, *J. Am. Chem. Soc. 91*, 726−731.
50. Byrd, J., Berger, R. M., McMillin, D. R., Wright, C. F., Hamer, D., and Winge, D. R. (1988) Characterization of the copper-thiolate cluster in yeast metallothionein and two truncated mutants, *J. Biol. Chem. 263*, 6688−6694.
51. Hasler, D. W., Faller, P., and Vasak, M. (1998) Metal−thiolate clusters in the C-terminal domain of human neuronal growth inhibitory factor (GIF), *Biochemistry 37*, 14966−14973.
52. Nielson, K. B., Atkin, C. L., and Winge, D. R. (1985) Distinct metal-binding conformations in metallothionein, *J. Biol. Chem. 260*, 5342−5350.
53. Nielson, K. B., and Winge, D. R. (1984) Preferential binding of copper to the β domain of metallothionein, *J. Biol. Chem. 259*, 4941−4946.
54. Poutney, D. L., Schauwecker, I., Zarn, J. W., and Vasak, M. (1994) Formation of mammalian Cu_8-metallothionionein in vitro: Evidence for the existence of two $Cu(I)_4$-thiolate clusters, *Biochemistry 33*, 9699−9705.
55. Formica-Kozlowski, G., Kozlowska, H., Siemion, I. Z., Sobczyk, K., and Nawrocka, E. (1984) The coordination of copper(II) with β-casomorphin and its fragments, *J. Inorg. Biochem. 22*, 155−163.
56. Pettit, L. D., Bataille, M., Gregor, J. E., and Kozlowska, H. (1991) Complex formation between metal ions and peptides, in *Perspectives on Bioinorganic Chemistry* (Hat, R. W., Dilworth, J. R., and Noland, K. B., Eds.) pp 1−41, JAI Press Ltd., Greenwich, CT.
57. Yamauchi, O., Tsujide, K., and Odani, A. (1985) Copper(II) complexes of tyrosine-containing dipeptides. Effects of side chain groups on spectral and solution chemical properties and their structural implications, *J. Am. Chem. Soc. 107*, 659−666.
58. Becker, R. S. (1969) *Theory and Interpretation of Fluorescence and Phosphorescence*, John Wiley & Sons, Inc., New York.
59. Guilbault, G. G. (1967) *Fluorescence Theory, Instrumentation, and Practice*, Marcel Dekker, New York.
60. Lakowicz, J. R. (1999) *Principles of Fluorescence Spectroscopy*, 2nd ed., Kluwer Academic/Plenum Publishers, New York.
61. Schulman, S. G. (1977) *Fluorescence and Phosphorescence Spectroscopy; Physiolochemical Principles and Practice*, Pergamon Press, Inc., New York.
62. Valeur, B. (2002) *Molecular Fluorescence*, Wiley-VCH, Weinheim, Germany.
63. Fasman, G. D. (1996) *Circular Dichroism and the Conformational Analysis of Biomolecules*, Plenum Press, New York.
64. Kowalik-Jankowska, T., Ruta-Dolejsz, M., Wisniewska, K., and Lankiewicz, L. (2002) Coordination of copper(II) ions by the 11−20 and 11−28 fragments of human and mouse β-amyloid peptide, *J. Inorg. Biochem. 92*, 1−10.
65. Berova, N., Nakanishi, K., and Woody, R. W. (2000) *Circular Dichroism*; *Principles and Applications*, 2nd ed., Wiley-VCH, New York.
66. Bain, C. D., Biebuyck, A., and Whitesides, G. M. (1989) Comparison of self-assembled monolayers on gold: Coadsorption of thiols and disulfides, *Langmuir 5*, 725−727.
67. Riga, J., and Verbist, J. J. (1983) The Disulphide Group in Organic Compounds: Conformational Dependence of Core and Valence Sulphur Electronic Levels by X-ray Photoelectron Spectroscopy, *J. Chem. Soc., Perkin Trans. 2*, 1545−1553.
68. Wagner, C. D., Naumkin, A. V., Kraut-Vass, A., Allison, J. W., Powell, C. J., and Rumble, J. R. J. (2005) U.S. National Institute of Standards and Technology.
69. Singh, R., Blatler, W. A., and Collinson, A. R. (1993) An amplified assay for thiols based on reactivation of papain, *Anal. Biochem. 91*, 49−56.
70. Martin, R. B. (1977) Complexes of α-amino acids with chelatable side chain donor atoms, *Ions Biol. Syst. 9*, 1−40.
71. May, P. M., and Williams, D. A. (1981) Role of low molecular weight copper complexes in the control of rheumatoid arthritis, *Met. Ions Biol. Syst. 12*, 283−317.
72. Pettit, L. D., and Hefford, R. J. W. (1979) Stereoselectivity in the metal complexes of amino acids and dipeptides, *Met. Ions Biol. Syst. 9*, 173−212.
73. Smith, R. M., and Martell, A. E. (1975) *Critical Stability Constants*, Vol. 2, Plenum Press, New York.
74. Smith, R. M., and Martell, A. E. (1989) *Critical Stability Constants*, Vol. 6, Plenum Press, New York.
75. Martell, A. E., and Smith, R. M. (1984) *Critical Stability Constants*, Vol. 1, Plenum Press, New York.
76. Burns, C. S., Aronoff-Spencer, E., Legname, G., Prusiner, S. B., Antholine, W. E., Gerfen, G. J., Peisach, J., and Millhauser, G. L. (2003) Cooper coordination in the full-length, recombinant prion protein, *Biochemistry 42*, 6794−6803.
77. Morante, S., Gonzalez-Igesias, A., Potrich, C., Meneghin, C., Meyer-Klaucke, W., Menestrain, G., and Gasset, M. (2004) Inter- and intra-octarepeat Cu(II) site geometries in the prion protein, *J. Biol. Chem. 279*, 11753−11759.
78. Wong, B.-S., Venien-Bryan, C., Williamson, R. A., Burton, D. R., Gambetti, P., Sy, M.-S., Browin, D. R., and Jones, I. M. (2000) Copper refolding of prion protein, *Biochem. Biophys. Res. Commun. 267*, 1217−1224.

BI051815T